Solving the conundrum of extensional folding in metamorphic core complexes

Dazhi Jiang[1,2,*] and Changcheng Li[1,†]

[1]Department of Earth Sciences, Western University, London, Ontario, Canada, N6A 5B7

[2]Department of Geology, Northwest University, Xi'an, China

† Current Address: Department of Earth and Environmental Sciences, University of Waterloo, Waterloo, Ontario, Canada N2L 3G1

*Correspondence to: djiang3@uwo.ca

Folds with axial traces parallel to the extension direction are a common feature in continental detachment systems and metamorphic core complexes. Yet, how they form has been puzzling for many decades. Here, we show that the key to solving the conundrum lies in revising the long-held single-scale view toward natural deformation and application of kinematic models. We demonstrate that extensional folding can result naturally from the partitioned stress field in competent layers in plate-scale extension and transtension deformations. Competent layers that develop extension folds should be regarded as rheological inclusions in the lithosphere rather than infinitely extending plates clamped at system boundaries and subjected to system boundary conditions.

In western North America Cordillera metamorphic core complexes, upright and open folds parallel to the extension direction are a common feature [1-6]. They fold detachment shear zones, mylonitic foliations and layering of the upper and lower plate rocks near the detachment shear zone (Fig.1a). Similar folds are also well developed in the high-grade nappe association of the southwestern Grenville Province in Ontario and western Quebec (Fig.1b) where they folded a subhorizontal foliation and compositional layering produced by an earlier crustal thickening deformation [7,8]. Despite their common occurrence, the origin of extension folds remains puzzling [4-6]. Field evidence suggests strongly that they are buckle folds developed during extension [4,6,9,10] and theoretical analysis [4] indicates that horizontal compression perpendicular to extension is required. However, there has been no generally-accepted geodynamic models to explain this horizontal compression, even though it is often invoked [11-13]. Recently, many people have recourse to transtension (oblique divergence; Fig.2a) [9,13]. However, as we show in more detail in the Supplementary Information, transtension can produce very limited horizontal shortening, regardless of the finite strain of the system (Fig.2b), if the divergence angle (ϕ in Fig.2a) is small. North America Cordillera metamorphic complexes indeed have very small divergence angles and

so is the western Grenville Province (Fig.1). The strains reflected by extension folds cannot be explained by the transtension model.

Here, we demonstrate that the difficulty in understanding extensional folding is due to our single-scale approach toward lithosphere deformation. We think it is unrealistic to regard layers that develop extension folds as infinitely-extending elastic or viscous plates that are subjected to the system boundary conditions. It is more realistic to regard them as rheologically heterogeneous inclusions embedded in the lithospheric mass undergoing macroscale transtension. It is the partitioned stress and strain field in these layers, rather than the homogenized stress and strain field of the macroscale transtension, that is relevant for extensional folding. We show that partitioned stress field can produce extension folds in competent layers in extension and transtension settings.

Partitioned stress field in a competent layer-like inclusion

Eshelby's inclusion solution [14-16] relates the stress and strain field inside an ellipsoid inclusion to the uniform macroscale field by:

$$\boldsymbol{\sigma} - \boldsymbol{\Sigma} = \mathbf{C} : \left(\mathbf{J}^s - \mathbf{S}^{-1} \right) : \left(\boldsymbol{\varepsilon} - \mathbf{E} \right) \qquad (1)$$

where $\mathbf{J}^s$ is the 4th-order identity tensor defined in terms of Kronecker delta, $J^s_{ijkl} = \frac{1}{2}\left(\delta_{ik}\delta_{jl} + \delta_{jk}\delta_{il} \right)$, lowercase $\boldsymbol{\sigma}$ and $\boldsymbol{\varepsilon}$ are the stress and strain (or strain rate) tensors in the inclusion, uppercase $\boldsymbol{\Sigma}$ and $\mathbf{E}$ are macroscale stress and strain (or strain rate) tensors in the matrix. Where both the inclusion and matrix are elastic (an all-elastic system), $\boldsymbol{\varepsilon}$ and $\mathbf{E}$ are elastic strains. Where both the inclusion and the matrix are Newtonian viscous (an all-viscous system), $\boldsymbol{\varepsilon}$ and $\mathbf{E}$ are strain rates. Where the matrix is viscous and the inclusion elastic, $\boldsymbol{\varepsilon}$ is elastic strain tensor of the inclusion and $\mathbf{E}$ the viscous strain rate tensor of the matrix. $\mathbf{C}$ is the elastic or viscous stiffness of the matrix depending on its rheology and $\mathbf{S}$ the Eshelby tensor for the inclusion.

We use the fundamental interaction equation (1) and the equivalent-inclusion approach [14,17] to derive analytical solutions for the partitioned stress in competent layer-like elements under macroscale transtension. The following assumptions are made. First, we regard the competent layer as a flat oblate inclusion with principal semi-axes $a_1 = a_2 >> a_3$. By varying the aspect ratio $\omega = \frac{a_3}{a_1}$, the inclusion may represent different bodies including a uniformly-thick plate ($\omega \to 0$). We believe that, on the macroscale suitable for continental transtension, no geological unit is

rheologically continuous throughout the deformation zone and subjected to the system boundary conditions. Second, for simplicity we assume that the rheology of the lithosphere on the macroscale and that of the inclusion are linear, isotropic, and incompressible. Third, on the macroscale appropriate for transtension, the lithosphere is approximated by a Homogeneous-Equivalent Medium (HEM) whose rheology is represented by the homogenized rheology of all the rheological elements in the macroscale representative volume [15,16,18,19]. We use the convention of tensile stress being positive so that tensile normal stress corresponds to positive extension strain.

To model extension folds in North America Cordillera metamorphic core complexes, we consider stress partitioning in an all-elastic system. Equation (1) leads to a strain partitioning equation $\boldsymbol{\varepsilon} = \left[\mathbf{J}^d + (r-1)\mathbf{S}\right]^{-1} : \mathbf{E}$ (ref.[15]) which, upon using Hooke's law, is rewritten in the following stress partitioning form:

$$\boldsymbol{\sigma} = r\left[\mathbf{J}^d + (r-1)\mathbf{S}\right]^{-1} : \boldsymbol{\Sigma} \tag{2}$$

where r is the ratio of the elastic shear modulus of the element μ to that of the HEM μ_s and $r = \dfrac{\mu}{\mu_s} > 1$ for competent layers; $\mathbf{J}^{\mathrm{d}}$ is the 4th-order deviatoric identity tensor defined as: $J^d_{ijkl} = J^s_{ijkl} - \dfrac{1}{3}\delta_{ij}\delta_{kl}$. Because the Eshelby tensor components for flat oblate inclusions ($a_1 = a_2 >> a_3$, $\omega = \dfrac{a_3}{a_1} << 1$) in linear incompressible materials can be obtained from elastic Eshelby tensors given in ref.[20], with a slightly tedious but otherwise straightforward derivation (Supplementary Information), we get the following expressions from equation (2) for the partitioned stress field in the element:

$$\sigma_{11} = \frac{2r\left\{\left[16 + 9\pi\omega(r-1)\right]\Sigma_{11} - 3\pi\omega(r-1)\Sigma_{22}\right\}}{\left[8 + 3\pi\omega(r-1)\right]\left[4 + 3\pi\omega(r-1)\right]} \tag{3a}$$

$$\sigma_{22} = \frac{2r\left\{\left[16 + 9\pi\omega(r-1)\right]\Sigma_{22} - 3\pi\omega(r-1)\Sigma_{11}\right\}}{\left[8 + 3\pi\omega(r-1)\right]\left[4 + 3\pi\omega(r-1)\right]} \tag{3b}$$

$$\sigma_{33} = \frac{4r\Sigma_{33}}{4 + 3\pi\omega(r-1)} \tag{3c}$$

$$\sigma_{12} = \frac{8r\Sigma_{12}}{8+3\pi\omega\left(r-1\right)} \tag{3d}$$

$$\sigma_{3\alpha} = \frac{4r\Sigma_{3\alpha}}{4r+3\pi\omega\left(r-1\right)}, \qquad (\alpha = 1,2) \tag{3e}$$

To model extension folds in the high metamorphic grade rocks in the Grenville Province, we regard the HEM as a Newtonian viscous material. The competent layers that develop extension folds may also be viscous, with a higher viscosity than the HEM. In such a case, the above results (equations (3)) can be applied if r in the equations is taken as the viscosity ratio between the inclusion and the HEM. We consider an additional situation where the element is instantaneously elastic; infinitesimal elastic strains of the layer are converted to permanent strains continually to give rise to the observed folds. In such a scenario, we apply the equivalent-inclusion approach to equation (1) by substituting the elastic inclusion with a fictitious inclusion of the same rheology as the HEM but with the same internal stress as the elastic inclusion. The interaction equation (1) becomes $\boldsymbol{\sigma}-\boldsymbol{\Sigma} = 2\eta_s\left(\mathbf{J}^d-\mathbf{S}^{-1}\right):\left(\frac{1}{2\mu}\frac{d\boldsymbol{\sigma}}{dt}-\frac{\boldsymbol{\Sigma}}{2\eta_s}\right)$, where, as in equation (2), μ is the shear modulus of the elastic inclusion; η_s is the HEM viscosity. This equation can be rearranged into a simpler form:

$$\left(\mathbf{J}^d-\mathbf{S}\right)\frac{d\boldsymbol{\sigma}}{d\hat{t}}+\mathbf{S}\boldsymbol{\sigma} = \boldsymbol{\Sigma} \tag{4}$$

where $\hat{t} = \frac{\mu}{\eta_s}t$ is the dimensionless time measured in unit of $\frac{\eta_s}{\mu}$, the characteristic viscoelastic relaxation time for the inhomogeneity and HEM interaction. Again, because Eshelby tensor components are all known, we can solve equation (4) (see Supplementary Information) to get:

$$\sigma_{11}\left(\hat{t}\right) = \frac{2}{3\pi\omega}\left[2\left(\Sigma_{11}-\Sigma_{22}\right)E_1\left(\hat{t}\right)+\left(\Sigma_{11}+\Sigma_{22}\right)E_2\left(\hat{t}\right)\right] \tag{5a}$$

$$\sigma_{22}\left(\hat{t}\right) = \frac{2}{3\pi\omega}\left[\left(\Sigma_{11}+\Sigma_{22}\right)E_2\left(\hat{t}\right)-2\left(\Sigma_{11}-\Sigma_{22}\right)E_1\left(\hat{t}\right)\right] \tag{5b}$$

$$\sigma_{33}\left(\hat{t}\right) = \frac{4\Sigma_{33}}{3\pi\omega}E_2\left(\hat{t}\right) \tag{5c}$$

$$\sigma_{12}\left(\hat{t}\right) = \frac{8\Sigma_{12}}{3\pi\omega}E_1\left(\hat{t}\right) \tag{5d}$$

$$\sigma_{3\alpha}\left(\hat{t}\right)=\frac{4\Sigma_{3\alpha}}{4-3\pi\omega}\left[1-\exp\left(-\frac{4-3\pi\omega}{3\pi\omega}\hat{t}\right)\right],\ \alpha=1,2 \tag{5e}$$

where $E_1\left(\hat{t}\right)=1-\exp\left(-\frac{3\pi\omega}{8-3\pi\omega}\hat{t}\right)$ and $E_2\left(\hat{t}\right)=1-\exp\left(-\frac{3\pi\omega}{4-3\pi\omega}\hat{t}\right)$.

Folding of a horizontal competent layer in transtension

The macroscale stress tensor for transtension, expressed in the coordinate system xyz (Fig.2a), is of the following form (see Supplementary Information):

$$\Sigma_{ij}=\begin{pmatrix}\Sigma_{11} & \Sigma_{12} & 0\\ \Sigma_{12} & 0 & 0\\ 0 & 0 & -\Sigma_{11}\end{pmatrix} \tag{6}$$

where the shear and normal stress components are related to the divergence angle by $\tan\phi=\frac{2\Sigma_{12}}{\Sigma_{11}}$. Submitting the stress expression in equation (6) into equations (3) and (5), we get the expressions for the partitioned deviatoric stress tensor in a horizontal flat oblate element for an all-elastic (or all-viscous) system and an elastic element in a viscous HEM, under macroscale transtension. Taking the eigenvalues, the corresponding principal stresses for an all-elastic system are:

$$\sigma_1=2r\Sigma_{11}\left[\frac{1}{4+3\pi\omega\left(r-1\right)}+\frac{2\sec\phi}{8+3\pi\omega\left(r-1\right)}\right] \tag{7a}$$

$$\sigma_2=2r\Sigma_{11}\left[\frac{1}{4+3\pi\omega\left(r-1\right)}-\frac{2\sec\phi}{8+3\pi\omega\left(r-1\right)}\right] \tag{7b}$$

$$\sigma_3=-\frac{4r\Sigma_{11}}{4+3\pi\omega\left(r-1\right)} \tag{7c}$$

and those for an elastic layer in a viscous HEM are:

$$\sigma_1\left(\hat{t}\right)=\frac{2\Sigma_{11}}{3\pi\omega}\left[E_2\left(\hat{t}\right)+2\sec\phi E_1\left(\hat{t}\right)\right] \tag{8a}$$

$$\sigma_2\left(\hat{t}\right)=\frac{2\Sigma_{11}}{3\pi\omega}\left[E_2\left(\hat{t}\right)-2\sec\phi E_1\left(\hat{t}\right)\right] \tag{8b}$$

$$\sigma_3\left(\hat{t}\right)=-\frac{4\Sigma_{11}}{3\pi\omega}E_2\left(\hat{t}\right) \tag{8c}$$

Note equations (8) do not breakdown at ω =0 because $\lim_{\omega\to 0}\frac{E_1\left(\hat{t}\right)}{\omega}=\frac{3\pi\hat{t}}{8}$ and $\lim_{\omega\to 0}\frac{E_2\left(\hat{t}\right)}{\omega}=\frac{3\pi\hat{t}}{4}$. The case of ω =0 means that the competent layer is an infinitely-extending sheet, and the solution converges to the single-scale solution of a horizontal sheet under macroscale transtension. In reality, a competent layer is an inclusion which means that ω is small but not zero.

It can be readily confirmed that the principal partitioned stress axes are parallel to the macroscale principal stresses for both equations (7) and (8). Therefore, whether treated as an all-elastic system, an all-viscous system, or as elastic layers in a viscous HEM, the partitioned principal stresses in a horizontal layer are parallel to the macroscale principal stresses but are increased in magnitude by approximately a factor of r or ω^{-1}. Significantly, the horizontal σ_2 is always compressive and does not vanish (equations (7b) and (8b)) even if the system is in pure extension ($\phi = 0^{\circ}; \Sigma_2 = 0$), unless ω =0.

As there are no available analytical solutions for the buckling of a flat oblate element embedded in an elastic or viscous matrix, we use the theory of cylindrical buckling of a rectangular elastic plate under in-plate loading [21,22] to provide an approximate analysis of a horizontal elastic layer element in an elastic or viscous HEM under transtension.

The tendency for a competent elastic layer to buckle is determined by its flexural rigidity [21], which for an incompressible elastic plate is $D=\frac{\mu h^3}{3}$ (h the thickness of the plate). The analysis in refs.[21,22] shows that the critical load P for the layer to buckle is $P=\frac{\pi^2}{L^2}D$ (L being the width of the elastic plate , ref.[21], p.132; ref.[22], p.119). For our situation, we can take $\frac{h}{L}\approx\omega$ and $P\approx-\left[\sigma_2-\left(\sigma_1+\sigma_3\right)\right]h=-2\sigma_2 h$. This yields an estimate for the critical σ_2 for buckling instability to develop in the layer:

$$\left|\sigma_2\right|_c=\frac{\pi^2\omega\mu}{6} \qquad (9)$$

According to equation (8b), σ_2 increases in magnitude asymptotically to $|\sigma_2| = \frac{2\Sigma_{11}(2\sec\phi - 1)}{3\pi\omega}$.

The critical aspect ratio for a horizontal layer is $\omega_c = \sqrt{\frac{4\Sigma_{11}(2\sec\phi - 1)}{\pi^3 \mu}}$. Similarly, in an all-elastic (or all viscous) system, we can use equation (7b) to find the critical aspect ratio. In the pure extension situation, the critical aspect ratio for a horizontal layer to develop buckling is $\omega'_c = \frac{4}{3\pi(r-1)}\left(\sqrt{1+\frac{18E_1}{\pi}(r-1)} - 3\right)$. Thus, all horizontal layer elements with aspect ratios $\omega < \omega_c$ or $\omega < \omega'_c$, depending on the rheologies considered, will eventually reach the critical compression for buckling and develop extension folds in transtension (Fig.3). Folding of a layer increases its effective aspect ratio. The folding of a layer will continue until the effective aspect ratio is below the critical value.

Folding of an inclined competent layer-like inclusion in transtension

Equations (3) and Equations (5) are applicable to an inclined layer in transtension, if the macroscale stress tensor components are expressed in the coordinate system of the inclusion. We note that in an inclined competent layer, the shear stresses $\sigma_{3\alpha}$ ($\alpha = 1, 2$) parallel to the layer do not vanish but are small compared to other σ_{ij} components. All σ_{ij} components are increased in magnitude by a factor of r or ω^{-1} from equivalent macroscale stresses except for $\sigma_{3\alpha}$ (equations (3) and (5)) which remain at the same level or smaller than the macroscale components ($\sigma_{3\alpha} \le \Sigma_{3\alpha}$). Therefore, in a strongly competent layer, $\sigma_{3\alpha}$ may be negligible compared to other components. This means that two of the three principal partitioned stress axes are always nearly parallel to the layer and the third principal stress is normal to the layer, despite of the layer orientation. This stress state is consistent with the field observation that competent layers are more prone to buckling and boudinage instabilities to develop folds and boudinage structures. It also implies that the classical elastic plate theory is a reasonable approximation for the deformation of thin competent layers in transtension.

We denote the strike and dip of an inclined competent layer by θ and δ respectively. It turns out that the orientation of the partitioned principal stresses in a competent layer is

independent of whether the system is all-elastic, all-viscous, or an elastic layer in a viscous HEM. The trend and plunge of σ_1-axis in a competent layer are expressed by (Supplementary Information):

$$\begin{aligned} \text{Trend} &= \frac{\pi}{2} + \theta - \tan^{-1}\left(\sec\delta \tan\psi\right) \\ \text{Plunge} &= \tan^{-1}\left\{\tan\delta \cos\left[\tan^{-1}\left(\sec\delta \tan\psi\right)\right]\right\} \end{aligned} \tag{10}$$

where $\psi = 0.5\tan^{-1}\left[\dfrac{2\sin\left(2\theta+\phi\right)\cos\delta}{\cos\left(2\theta+\phi\right)\left(1+\cos^2\delta\right)-3\cos\phi\sin^2\delta}\right]$ and θ is measured with respect to the y-axis (Fig.2a).

If buckling folds initiate in the layer parallel to σ_1-axis, we can use equation (10) to predict the initial orientations of folds in a transtension deformation. Fig. 4 plots the expected initial fold hinge lines in competent layers of varying dip angles in a transtension of $\phi = 30^\circ$. Two different types of folds may develop. Horizontal to moderately-dipping competent layers (e.g., dip between 0 and 30°) will develop upright extension folds, if their aspect ratios ω are sufficiently small. Steeply-dipping competent layers will buckle to form shallowly-plunging folds with subhorizontal axial surfaces. These folds are not the extension folds discussed in this paper. The initial trends of the fold hinge lines are controlled by the strike of the competent layer. Fold hinge lines will rotate toward the divergence vector.

Discussion and concluding remarks

The concept of stress (and strain) is not a single-scale quantity in a rheologically heterogeneous material like Earth's lithosphere. In a plate-scale deformation such as transtension, the corresponding macroscale Σ_{ij} are homogenized stresses on a large representative volume suitable for the bulk deformation. They are distinct from the partitioned stresses σ_{ij} in a specific rheological element, such as a competent layer, in which extension folds develop. If one uses a single-scaled Σ_{ij} (or associated strain field) to consider the development of extension folds, one runs into a conundrum, because Σ_2 is zero or very small in the event of pure extension or transtension with a small ϕ. The single-scaled use of Σ_{ij} amounts to regarding a layer in which extension folds develop as a continuous sheet extending throughout the transtension zone and

being subjected to the macroscale transtension boundary conditions. No geological layers are *rheologically* continuous on such macroscale suitable for transtension deformation. They are more realistically treated as layer-like inclusions in the lithosphere mass on that scale. Folding of such an element must then be considered in terms of the partitioned stress field.

All geological structures in Earth's lithosphere, not just extension folds in transtension, develop in rheologically distinctive elements in the lithosphere. They are thus related to the partitioned stress σ_{ij} not the homogenized Σ_{ij}. The significance of stress partitioning in Earth's lithosphere as we highlighted here raises issues with many current practices based on the single-scale conception. The use of paleo-stress estimates from mylonite shear zones as a proxy of stress in the lithosphere [23] is an example. Ductile shear zones are essentially rheologically weak (lower effective viscosity) inclusions in the lithosphere (the $r<1$ case of equation (2)). Equation (2) suggests that σ_{ij} in a mylonite shear zone are likely distinct from and smaller in magnitude than Σ_{ij} of the bulk lithosphere making it unjustified to assume that $\sigma_{ij} \approx \Sigma_{ij}$ or that the invariants of the two are approximately equal.

References

1 John, B. E. Geometry and evolution of a mid-crustal extensional fault system: Chemehuevi Mountains, southeastern California. *Geological Society, London, Special Publications* **28**, 313-335, (1987).

2 Davis, G. A. & Lister, G. S. Vol. 218 (eds S. P. Clark, Jr., B. C. Burchfiel, & J. Suppe) 133-159 (Geological Society of America, 1988).

3 Spencer, J. E. & Reynolds, S. J. Tectonics of Mid-Tertiary Extension along a transect through west central Arizona. *Tectonics* **10**, 1204-1221, (1991).

4 Yin, A. Mechanisms for the formation of domal and basinal detachment faults: a three-dimensional analysis. *Journal of Geophysical Research* **96**, 14,577-514,594, (1991).

5 Davis, G. A. *et al.* Pluton pinning of an active Miocene detachment fault system, eastern Mojave Desert, California *Geology* **21**, 627-630, (1993).

6 Fletcher, J. M. & Bartley, J. M. Constrictional strain in a non-coaxial shear zone: implications for fold and rock fabric development, central mojave metamorphic core complex, california. *Journal of Structural Geology* **16**, 555-570, (1994).

7 Culshaw, N. G., Ketchum, J. W. F., Wodicka, N. & Wallace, P. Deep crustal ductile extension following thrusting in the southwestern Grenville Province, Ontario. *Canadian Journal of Earth Sciences* **31**, 160-175, (1994).

8 Li, C. *An Investigation of Deformation Structures and Their Tectonic Significance Across the Grenville Front Tectonic Zone in the Vicinity of Sudbury, Ontario, Canada* Ph.D thesis, Western University, (2012).

9 Brown, S. R., Andrews, G. D. M. & Gibson, H. D. Corrugated architecture of the Okanagan Valley shear zone and the Shuswap metamorphic complex, Canadian Cordillera. *Lithosphere* **8**, 412-421, (2016).
10 Singleton, J. S. Development of extension-parallel corrugations in the Buckskin-Rawhide metamorphic core complex, west-central Arizona. *GSA Bulletin* **125**, 453-472, (2013).
11 Mancktelow, N. & Pavlis, T. *Fold-fault relationships in low-angle detachment systems*. Vol. 13 (1994).
12 Fletcher, J. M., Bartley, J. M., Martin, M. W., Glazner, A. F. & Walker, J. D. Large-magnitude continental extension: An example from the central Mojave metamorphic core complex. *GSA Bulletin* **107**, 1468-1483, (1995).
13 Schwerdtner, W. M. *et al.* Transtensional origin of multi-order cross-folds in a high-grade gneiss complex, southwestern Grenville Province: Formation during post-peak gravitational collapse. *Canadian Journal of Earth Sciences* **53**, 1511-1538, (2016).
14 Eshelby, J. D. The Determination of the Elastic Field of an Ellipsoidal Inclusion, and Related Problems. *Proceedings of the Royal Society of London. Series A, Mathematical and Physical Sciences* **241**, 376-396, (1957).
15 Jiang, D. Structural geology meets micromechanics: A self-consistent model for the multiscale deformation and fabric development in Earth's ductile lithosphere. *Journal of Structural Geology* **68**, 247-272, (2014).
16 Jiang, D. Viscous inclusions in anisotropic materials: Theoretical development and perspective applications. *Tectonophysics* **693**, 116-142, (2016).
17 Rudnicki, J. W. The inception of faulting in a rock mass with a weakened zone. *Journal of Geophysical Research (1896-1977)* **82**, 844-854, (1977).
18 Jiang, D. & Bentley, C. A micromechanical approach for simulating multiscale fabrics in large-scale high-strain zones: Theory and application. *Journal of Geophysical Research: Solid Earth* **117**, (2012).
19 Lebensohn, R. A. & Tomé, C. N. A self-consistent anisotropic approach for the simulation of plastic deformation and texture development of polycrystals: Application to zirconium alloys. *Acta Metallurgica et Materialia* **41**, 2611-2624, (1993).
20 Mura, T. *Micromechanics of Defects in Solids*. 587 (Dordrecht : Nijhoff, 1987).
21 Turcotte, D. L. & Schubert, G. *Geodynamics : Applications of Continuum Physics to Geological Problems*. 450 (Wiley, 1982).
22 Reddy, J. N. *Theory and analysis of elastic plates and shells*. 2nd edn, 568 (CRC Press, 2006).
23 Platt, J. P. & Behr, W. M. Lithospheric shear zones as constant stress experiments. *Geology* **39**, 127-130, (2011).
24 Kruckenberg, S. C., Whitney, D. L., Teyssier, C., Fanning, C. M. & Dunlap, W. J. Paleocene-Eocene migmatite crystallization, extension, and exhumation in the hinterland of the northern Cordillera: Okanogan dome, Washington, USAMigmatite crystallization and exhumation in the Okanogan dome, Washington. *GSA Bulletin* **120**, 912-929, (2008).
25 Okulitch, A. V. Comment on "Extension across the Eocene Okanagan crustal shear in southern British Columbia". *Geology* **15**, 187-188, (1987).
26 Davidson, A. Tectonic history of the Grenville Province, Ontario. (Geological Survey of Canada, 1995).
27 Lumbers, S. B. *Geology of the Burwash Area, Districts of Nipissing, Parry Sound, and Sudbury*. (Ontario Division of Mines, Geological report 116, 1975).

Acknowledgments: We are grateful to Lucy X. Lu, Ankit Bhandari, and Rui Yang for many discussions. We tank Lucy Lu for help with plotting Fig.4 using Matlab. This research is supported by Canada's Natural Science and Engineering Research Council (NSERC) through a Discovery Grant; China's National Natural Science Foundation (NSFC, grants 41472184 and 41772213), and Northwest University.

Author contributions: DJ developed the theory, derived all the equations, and wrote the paper. CL conducted field structural analysis in the Grenville Front region and prepared Fig.1. Both were involved with the interpretation of field data and discussion of the ideas of the paper.

Competing interests: Authors declare no competing interests.

Data and materials availability: All data is available in the main text or the supplementary materials.

Additional information

Supplementary Text

Figure S1

Supplementary References

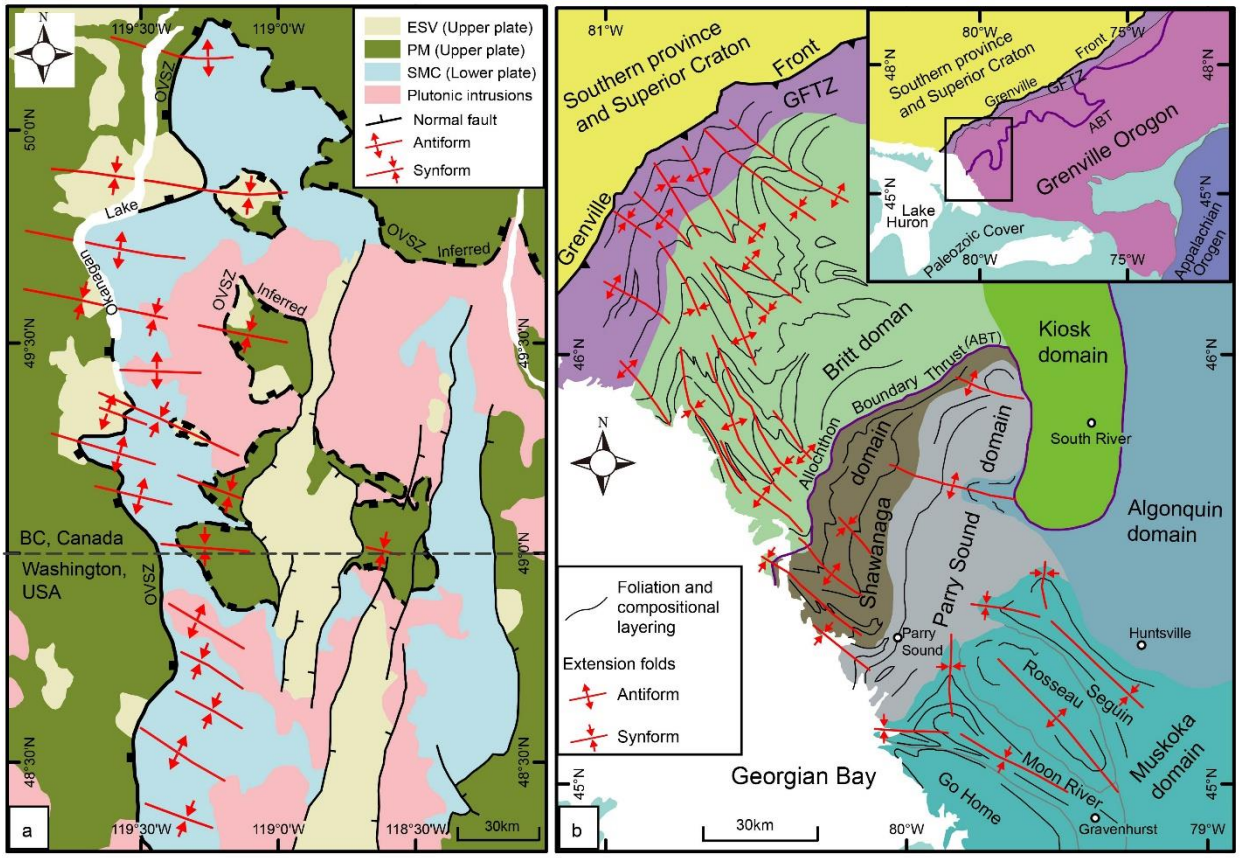

Fig. 1: Extension folds are common in continental divergence settings.

a, Simplified geological map of the Okanagan Valley shear zone (OVSZ) and the Shuswap metamorphic complex (SMC) of the Canadian Cordillera showing upright and open extension folds throughout the system. These folds formed during extension (ca.54-48Ma) and are nearly orthogonal to the overall strike of the system. PM: Paleozoic & Mesozoic rocks; ESV: Eocene sedimentary and volcanic rocks. Figure is adapted from refs.[9,24,25]. **b**, Simplified map showing extension upright folds formed ~ca.1020Ma in the high-grade nappe association in southwestern Grenville Province in Ontario and western Quebec. The surfaces being folded by the extension folds are a subhorizontal layering and transposition foliation produced during an earlier (~1070-1030Ma) crustal thickening [7,8]. The fold hinge lines are nearly orthogonal to the Grenville Front which is the northwest boundary of the Grenville Orogen. In the Grenville Front Tectonic Zone (GFTZ), the folds have been overprinted by the ca.1000-975Ma shear zones. The upper-right index map shows the broader context. Map is compiled from refs.[7,8,26,27].

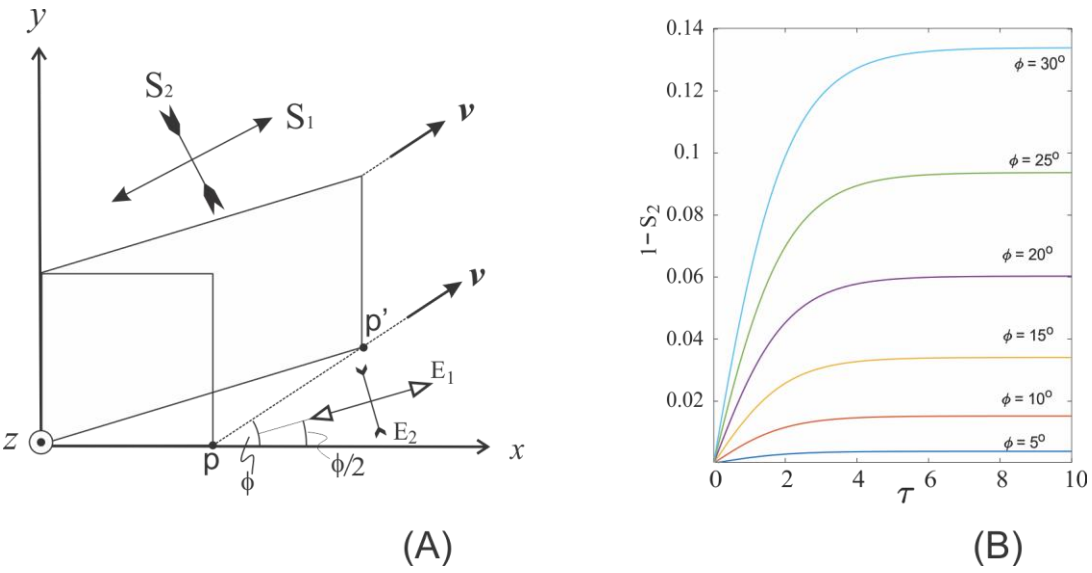

Fig. 2: Map view of macroscale transtension and strain in the horizontal plane.

a, Transtension geometry and coordinate system xyz used to define the deformation. The horizontal divergence vector **v** is at an angle ϕ relative to the system normal (the x- axis). An initial square is deformed progressively into a parallelogram with its lower-right corner (p) moving along **v** (dashed line to the final position p'). The horizontal principal stretching (E_1) axis is at $\frac{\phi}{2}$ relative to the x- axis and the horizontal principal shortening E_2-axis is normal to E_1-axis. They also are parallel to the two horizontal principal stresses Σ_1 and Σ_2 (not shown in Figure but referred to in text). The two horizontal principal finite strains, measured by stretch, are $S_1 > S_2$ and S_1 orientation is between E_1-axis and **v** depending on the magnitude of finite strain. **b**, When ϕ is small, S_2 remains close to 1 regardless of the finite strain rendering minor horizontal principal shortening (1- S_2).

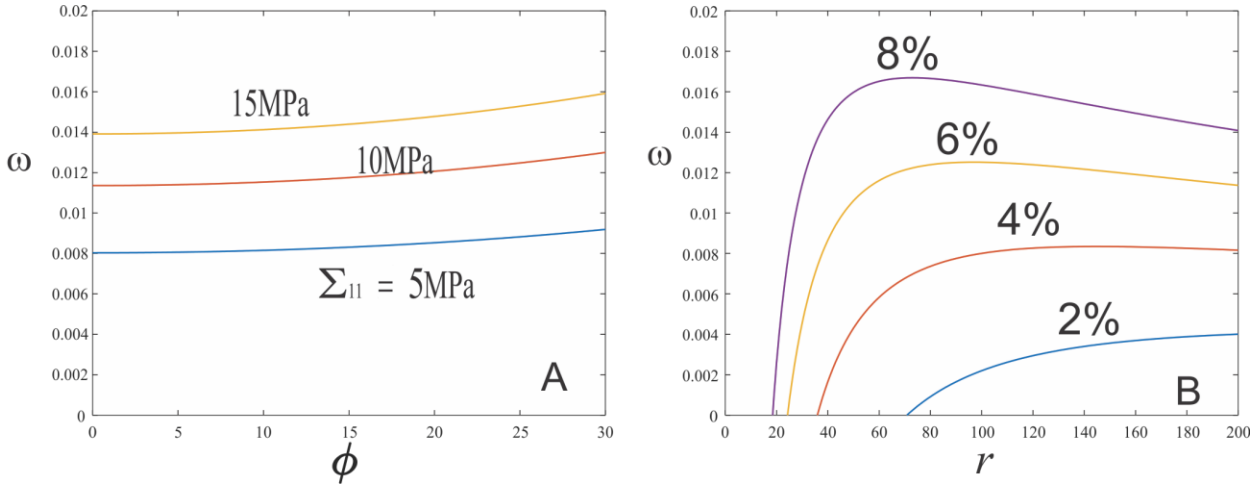

Fig. 3: Critical aspect ratios of buckling for a horizontal competent layer in transtension.

a, A competent elastic layer in an elastic HEM. For modest macroscale extension stress Σ_{11} between 5 and 15MPa, horizontal layer-like inclusions with $\omega < 0.015$ can buckle. **b**, A competent elastic layer in a viscous HEM. Different curves represent different macroscale elongation strain E_1.

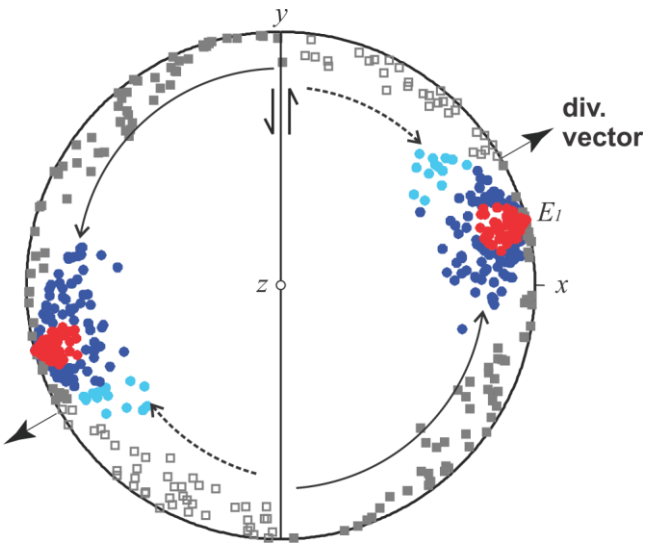

Fig. 4: Initial orientations of buckling folds in inclined competent layers in a transtension with $\phi = 30^{\circ}$. Red dots are fold hinge lines in competent layers with dip angle between 0 and 20°; Dark and light blue dots are fold hinge lines in competent layers with dip angles between 20° and 40°. Upright extension folds are developed in these layers close to the principal extension E_1 axis. They may rotate with (dark blue dots) or against (light blue dots) the macroscale vorticity toward the divergence vector. In contrast, steeply-dipping to vertical competent layers with dip angles between 50° and 90° (squares) may buckle to develop shallowly-plunging folds, largely due to vertical compression. The initial fold hinge lines are determined by the strike of the layer. These folds have subhorizontal axial surfaces (recumbent folds) and are not the extension folds discussed in this paper. Nevertheless, they may occur in transtension. These folds may rotate with (solid squares) or against (open squares) the macroscale vorticity toward the divergence direction.

Supplementary Information

1. Transtension

The velocity gradient tensor for macroscale transtension considered in coordinate system xyz (Fig.2 in the text) can be expressed as:

$$L_{ij} = \frac{v}{d}\begin{pmatrix} \cos\phi & 0 & 0 \\ \sin\phi & 0 & 0 \\ 0 & 0 & -\cos\phi \end{pmatrix} \tag{s1}$$

where v is the divergence velocity, d the width of transtension, and ϕ the angle of divergence velocity measured relative to the transtension normal (the x-axis). The $\frac{v}{d}$ determines the rate of deformation while the kinematics of the deformation is fully determined by ϕ. The associated strain rate tensor is

$$E_{ij} = \frac{1}{2}\left(L_{ij} + L_{ji}\right) = \frac{v}{d}\begin{pmatrix} \cos\phi & 0.5\sin\phi & 0 \\ 0.5\sin\phi & 0 & 0 \\ 0 & 0 & -\cos\phi \end{pmatrix} \tag{s2}$$

which for a macroscale isotropic lithosphere with viscosity η_s corresponds to the following deviatoric stress tensor ($\Sigma_{ij} = 2\eta_s E_{ij}$):

$$\Sigma_{ij} = \begin{pmatrix} \Sigma_{11} & \Sigma_{12} & 0 \\ \Sigma_{12} & 0 & 0 \\ 0 & 0 & -\Sigma_{11} \end{pmatrix} \tag{s3}$$

And it can be readily verified that $\tan\phi = \frac{2\Sigma_{12}}{\Sigma_{11}}$.

Eq.s1 can be integrated (refs.[1,2]) to give the following position gradient tensor for transtension:

$$F_{ij}(\tau) = \begin{pmatrix} e^{\tau\cos\phi} & 0 & 0 \\ \tan\phi\left(e^{\tau\cos\phi} - 1\right) & 1 & 0 \\ 0 & 0 & e^{-\tau\cos\phi} \end{pmatrix} \tag{s4}$$

where τ is the dimensionless time, $\tau = \frac{v}{d}t$.

The three principal stretches are obtained (see ref.[2] for more detail) by taking the eigenvalues of the tensor $V_{ij} = F_{im}(\tau)F_{jm}(\tau)$. The three principal stretches are:

$$s_1(\phi,\tau) = \sqrt{h(\phi,\tau) + \mathrm{g}(\phi,\tau)} \tag{s5a}$$

$$s_2(\phi,\tau) = \sqrt{h(\phi,\tau) - \mathrm{g}(\phi,\tau)} \tag{s5b}$$

$$s_3(\phi,\tau) = e^{-\tau\cos\phi} \tag{s5c}$$

where $g(\phi,\tau)=\dfrac{\sec\phi\sqrt{\left(1+e^{4\tau\cos\phi}\right)\sec^2\phi-2e^{\tau\cos\phi}\left[e^{\tau\cos\phi}+\tan^2\phi\left(2-3e^{\tau\cos\phi}+2e^{2\tau\cos\phi}\right)\right]}}{2}$ and $h(\phi,\tau)=\dfrac{1}{2}\sec^2\phi\left(e^{\tau\cos\phi}-1\right)^2+e^{\tau\cos\phi}$. Fig. 2b in the text is based on Eq. s5b.

2. Inclined Competent Layer in Transtension

For an inclined inclusion with strike θ and dip angle δ, we set the inclusion coordinate system x'y'z' such that the x'-axis is along the dipline of the layer and pointing down, y'-axis is parallel to the strike of the layer, and z'-axis is normal to the layer and pointing up (Fig.S1). The rotation matrix Q_{ij} relating xyz and x'y'z' coordinates are [3]:

$$Q_{ij}=\begin{pmatrix}\cos\theta\cos\delta & -\sin\theta\cos\delta & -\sin\delta\\ \sin\theta & \cos\theta & 0\\ \cos\theta\sin\delta & -\sin\theta\sin\delta & \cos\delta\end{pmatrix} \tag{s6}$$

The macroscale stress tensor expressed in the inclusion coordinate system are obtained by tensor transformation $\Sigma'_{ij}=Q_{im}Q_{jn}\Sigma_{mn}$:

$$\Sigma'_{ij}=\begin{pmatrix}\Sigma_{11}\left(\cos^2\theta\cos^2\delta-\sin^2\delta\right)-\Sigma_{12}\sin 2\theta\cos^2\delta & \left(\Sigma_{11}\sin\theta\cos\theta+\Sigma_{12}\cos 2\theta\right)\cos\delta & 0.5\sin 2\delta\left[\Sigma_{11}\left(1+\cos^2\theta\right)-\Sigma_{12}\sin 2\theta\right]\\ \left(\Sigma_{11}\sin\theta\cos\theta+\Sigma_{12}\cos 2\theta\right)\cos\delta & \Sigma_{11}\sin^2\theta+\Sigma_{12}\sin 2\theta & \left(\Sigma_{11}\sin\theta\cos\theta+\Sigma_{12}\cos 2\theta\right)\sin\delta\\ 0.5\sin 2\delta\left[\Sigma_{11}\left(1+\cos^2\theta\right)-\Sigma_{12}\sin 2\theta\right] & \left(\Sigma_{11}\sin\theta\cos\theta+\Sigma_{12}\cos 2\theta\right)\sin\delta & \Sigma_{11}\left(\cos^2\theta\sin^2\delta-\cos^2\delta\right)-\Sigma_{12}\sin 2\theta\sin^2\delta\end{pmatrix} \tag{s7}$$

The partitioned stress tensor components are obtained by inserting Σ'_{ij} in place of Σ_{ij} in equations (3) and (5). In either case, the orientation of the σ_1-axis relative to x'-axis is:

$$\tan 2\psi=\frac{2\sigma_{12}}{\sigma_{11}-\sigma_{22}}=\frac{2\Sigma'_{12}}{\Sigma'_{11}-\Sigma'_{22}}=\frac{2\sin\left(2\theta+\phi\right)\cos\delta}{\cos\left(2\theta+\phi\right)\left(1+\cos^2\delta\right)-3\cos\phi\sin^2\delta} \tag{s8}$$

With ψ obtained from Eq.s8, the trend and plunge for σ_1-axis (equation (10) in text) can be obtained readily from simple trigonometry.

3. Derivation of Equations (3)

Elastic Eshelby tensor components are given in ref.[4] (p.81) for ellipsoid of general shapes with three semi-axes $a_1 \geq a_2 \geq a_3$. The corresponding Eshelby tensor components for incompressible materials can be calculated using the procedure of ref.[5]. Only components with indices S_{iijj} and S_{ijij} are not zero. For flat oblate inclusions ($a_1 = a_2 >> a_3$ and $\omega = \frac{a_3}{a_1} << 1$), the non-zero components are:

$$S_{iijj} = S_{ij} = \frac{\pi\omega}{16}\begin{pmatrix} 5 & -1 & -4 \\ -1 & 5 & -4 \\ -4 & -4 & 8 \end{pmatrix},\ S_{1313} = S_{2332} = \frac{1}{2}\left(1 - \frac{3\pi\omega}{4}\right), \text{ and } S_{1212} = \frac{3\pi\omega}{16} \qquad \text{(s9)}$$

To obtain equations (3) from equation (2), one needs to find explicit expressions for components of $\left[\mathbf{J}^d + (r-1)\mathbf{S}\right]^{-1}$ which involves inversion of 4th-order symmetrical tensors for isotropic and incompressible materials. Such tensors have the common property that all components are zero except A_{iijj} and A_{ijij} components. The A_{iijj} components and A_{ijij} components are obtained separately below. We make use of the contracted notation $A_{ij} = A_{iijj}$, such as $S_{ij} \equiv S_{iijj}$.

Denote $\mathbf{\Phi}(r) = \left[\mathbf{J}^d + (r-1)\mathbf{S}\right]$ and $\mathbf{\Psi}(r) = \mathbf{\Phi}^{-1}(r)$. The expression for $\Psi_{ijij}(r)$ is already given in ref.[5] as $\Psi_{ijij}(r) = \frac{1}{2\left[1 + 2(r-1)S_{ijij}\right]}$. It is only necessary to find expressions for $\Psi_{iijj}(r)$.

By definition $J^d{}_{ij} = J^d{}_{iijj} = \delta_{ij}\delta_{ij} - \frac{1}{3}\delta_{ii}\delta_{jj}$ (no sum) and $\Phi_{ij}(r) = \left[J^d{}_{ij} + (r-1)S_{ij}\right]$. Therefore, all $\Phi_{ij}(r)$ components are known for a given inclusion. Getting $\Psi_{ij} = \Psi_{iijj}$ is equivalent to solving the linear system: $\Phi_{ij}\begin{pmatrix} \varepsilon_{11} \\ \varepsilon_{22} \\ \varepsilon_{33} \end{pmatrix} = \begin{pmatrix} E_{11} \\ E_{22} \\ E_{33} \end{pmatrix}$. As the system is singular because of incompressible condition ($\varepsilon_{11} + \varepsilon_{22} + \varepsilon_{33} = E_{11} + E_{22} + E_{33} = 0$), it gives rise to the following non-singular subsystem

$$\begin{pmatrix} \Phi_{11} - \Phi_{13} & \Phi_{12} - \Phi_{13} \\ \Phi_{21} - \Phi_{23} & \Phi_{22} - \Phi_{23} \end{pmatrix}\begin{pmatrix} \varepsilon_{11} \\ \varepsilon_{22} \end{pmatrix} = \begin{pmatrix} E_{11} \\ E_{22} \end{pmatrix} \qquad \text{(s10)}$$

which can be readily solved:

$$\begin{pmatrix}\varepsilon_{11}\\ \varepsilon_{22}\end{pmatrix}=\Delta^{-1}\begin{pmatrix}\Phi_{22}-\Phi_{23} & \Phi_{13}-\Phi_{12}\\ \Phi_{23}-\Phi_{21} & \Phi_{11}-\Phi_{13}\end{pmatrix}\begin{pmatrix}E_{11}\\ E_{22}\end{pmatrix} \tag{s11}$$

where $\Delta=\left(\Phi_{11}-\Phi_{13}\right)\left(\Phi_{22}-\Phi_{23}\right)-\left(\Phi_{12}-\Phi_{13}\right)\left(\Phi_{21}-\Phi_{23}\right)$.

The ε_{33} component can be obtained by: $\varepsilon_{33}=-\left(\varepsilon_{11}+\varepsilon_{22}\right)$.

Submitting $\Phi_{ij}=\left[J^{d}{}_{ij}+(r-1)S_{ij}\right]$ to Eq.s11, one gets:

$$\Psi_{ij}(r)=\Delta^{-1}\begin{pmatrix}1+(r-1)\left(S_{22}-S_{23}\right) & -(r-1)\left(S_{12}-S_{13}\right) & 0\\ -(r-1)\left(S_{21}-S_{23}\right) & 1+(r-1)\left(S_{11}-S_{13}\right) & 0\\ -\left[1+(r-1)\left(S_{22}-S_{21}\right)\right] & -\left[1+(r-1)\left(S_{11}-S_{12}\right)\right] & 0\end{pmatrix} \tag{s12}$$

and $\Delta=\left[1+(r-1)\left(S_{11}-S_{13}\right)\right]\left[1+(r-1)\left(S_{22}-S_{23}\right)\right]-(r-1)^{2}\left(S_{12}-S_{13}\right)\left(S_{21}-S_{23}\right)$.

Submitting Eq.s9 into Eq.s12, we get the following expression for flat oblate inclusions:

$$\Psi_{ij}(r)=\frac{2}{\left[8+3\pi\omega(r-1)\right]\left[4+3\pi\omega(r-1)\right]}\begin{pmatrix}16+9\pi\omega(r-1) & -3\pi\omega(r-1) & 0\\ -3\pi\omega(r-1) & 16+9\pi\omega(r-1) & 0\\ -16-6\pi\omega(r-1) & -16-6\pi\omega(r-1) & 0\end{pmatrix} \tag{s13}$$

The explicit expressions for three normal stresses are, from equation (2):

$$\sigma_{ii}=r\Psi_{i\alpha}(r)\Sigma_{\alpha\alpha}\qquad\text{(sum over }\alpha\text{ only)} \tag{s14}$$

Expanding Eq.s14 gives Eqs.3a-c in the text.

The shear stresses can be readily obtained by $\sigma_{ij}=2\Psi_{ijij}\Sigma_{ij}=\dfrac{\Sigma_{ij}}{1+2(r-1)S_{ijij}}$ which gives equations (3d) and (3e) in the text.

4. Derivation of Equations (5)

For shear stresses σ_{ij} ($i\neq j$), we expand equation (6) as:

$$\left(1-2S_{ijij}\right)\frac{d\sigma_{ij}}{d\hat{t}}+2S_{ijij}\sigma_{ij}=\Sigma_{ij}\quad\text{(no sum)}$$

which can be solved to give $\sigma_{ij}\left(\hat{t}\right)=\dfrac{\Sigma_{ij}}{2S_{ijij}}\left[1-\exp\left(-\dfrac{2S_{ijij}}{1-2S_{ijij}}\hat{t}\right)\right]$. Inserting S_{ijij} for flat oblate inclusions (Eq.s9) gives:

$$\sigma_{12}\left(\hat{t}\right)=\frac{8\Sigma_{12}}{3\pi\omega}\left[1-\exp\left(-\frac{3\pi\omega}{8-3\pi\omega}\hat{t}\right)\right]=\frac{8\Sigma_{12}}{3\pi\omega}E_1\left(\hat{t}\right)$$
$$\sigma_{3\alpha}\left(\hat{t}\right)=\frac{4\Sigma_{3\alpha}}{4-3\pi\omega}\left[1-\exp\left(-\frac{4-3\pi\omega}{3\pi\omega}\hat{t}\right)\right] \qquad \text{(s15)}$$

which are equations (5d&e) in the text.

A different approach is used to solve for the three normal stresses σ_{ii} ($i=1,2,3$). First, we rewrite Eq.4 as $\frac{d\boldsymbol{\sigma}}{d\hat{t}}+\left(\mathbf{J}^d-\mathbf{S}\right)^{-1}\mathbf{S}\boldsymbol{\sigma}=\left(\mathbf{J}^d-\mathbf{S}\right)^{-1}\boldsymbol{\Sigma}$ first, and then in component form as:

$$\frac{d\sigma_{ii}}{d\hat{t}}+\Psi_{i\alpha}\left(0\right)S_{\alpha\beta}\sigma_{\beta\beta}=\Psi_{i\alpha}\left(0\right)\Sigma_{\alpha\alpha} \qquad \text{sum over Greek indices only} \qquad \text{(s16)}$$

$\Psi_{ij}\left(0\right)$ can be obtained from Eq.s13 and $S_{\alpha\beta}$ are given in Eq.s9. Submitting them into Eq.s16, the resulting equation can then be solved to give:

$$\sigma_{11}\left(\hat{t}\right)=\frac{2}{3\pi\omega}\left\{2\left(\Sigma_{11}-\Sigma_{22}\right)\left[1-\exp\left(-\frac{3\pi\omega}{8-3\pi\omega}\hat{t}\right)\right]+\left(\Sigma_{11}+\Sigma_{22}\right)\left[1-\exp\left(-\frac{3\pi\omega}{4-3\pi\omega}\hat{t}\right)\right]\right\} \qquad \text{(s17a)}$$

$$\sigma_{22}\left(\hat{t}\right)=\frac{2}{3\pi\omega}\left\{\left(\Sigma_{11}+\Sigma_{22}\right)\left[1-\exp\left(-\frac{3\pi\omega}{4-3\pi\omega}\hat{t}\right)\right]-2\left(\Sigma_{11}-\Sigma_{22}\right)\left[1-\exp\left(-\frac{3\pi\omega}{8-3\pi\omega}\hat{t}\right)\right]\right\} \qquad \text{(s17b)}$$

$$\sigma_{33}\left(\hat{t}\right)=\frac{4\Sigma_{33}}{3\pi\omega}\left[1-\exp\left(-\frac{3\pi\omega}{4-3\pi\omega}\hat{t}\right)\right] \qquad \text{(s17c)}$$

which are equations (5a-c) in the text.

For a horizontal flat oblate inclusion in transtension, inserting equation (4) into Eqs.s15 and s17, we get:

$$\sigma_{11}\left(\hat{t}\right)=\frac{2\Sigma_{11}}{3\pi\omega}\left[2E_1\left(\hat{t}\right)+E_2\left(\hat{t}\right)\right] \qquad \text{(s12a)}$$

$$\sigma_{22}\left(\hat{t}\right)=-\frac{2\Sigma_{11}}{3\pi\omega}\left[2E_1\left(\hat{t}\right)-E_2\left(\hat{t}\right)\right] \qquad \text{(s12b)}$$

$$\sigma_{33}\left(\hat{t}\right)=-\frac{4\Sigma_{11}}{3\pi\omega}E_2\left(\hat{t}\right) \qquad \text{(s12c)}$$

$$\sigma_{12}\left(\hat{t}\right)=\frac{8\Sigma_{12}}{3\pi\omega}E_1\left(\hat{t}\right) \qquad \text{(s12d)}$$

$$\sigma_{13}\left(\hat{t}\right)=\sigma_{23}\left(\hat{t}\right)=0 \qquad \text{(s12e)}$$

The corresponding principal stresses are equations (8) in text.

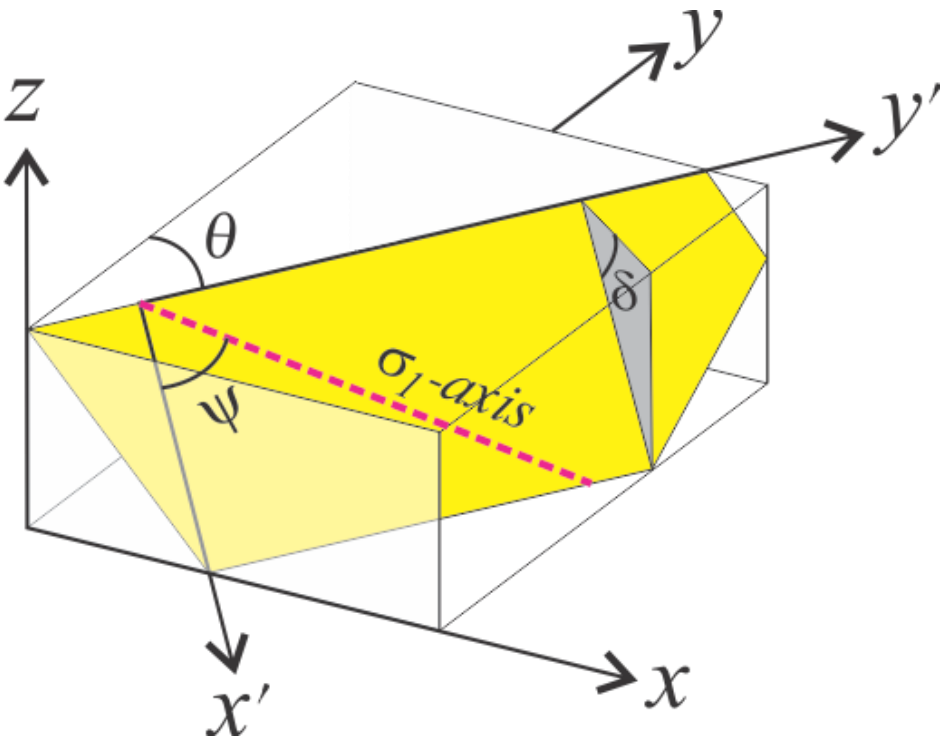

Fig. S1. Coordinate system x'y'z' for an inclined layer-like inclusion. Coordinate system xyz is the one in which macroscale transtension is defined. The yellow plane is the inclined layer, θ and δ are respectively strike and dip angles. The x'-axis is along the dipline of the layer and pointing down, y'-axis is parallel to the strike of the layer, and z'-axis (not shown) is normal to the layer and pointing up. ψ is the angle of the partitioned principal σ_1 axis relative to the x'-axis.

References:

1 Jiang, D. & Williams, P. F. High-strain zones: a unified model. *Journal of Structural Geology* **20**, 1105-1120, (1998).

2 Jiang, D. Flow and finite deformation of surface elements in three dimensional homogeneous progressive deformations. *Tectonophysics* **487**, 85-99, (2010).

3 Jiang, D. Numerical modeling of the motion of rigid ellipsoidal objects in slow viscous flows: A new approach. *Journal of Structural Geology* **29**, 189-200, (2007).

4 Mura, T. *Micromechanics of Defects in Solids*. 587 (Dordrecht : Nijhoff, 1987).

5 Jiang, D. Viscous inclusions in anisotropic materials: Theoretical development and perspective applications. *Tectonophysics* **693**, 116-142, (2016).